Microfluidic Colloidal Island Formation and Erasure Induced by Surface Acoustic Wave Radiation

Haiyan Li, James R. Friend, and Leslie Y. Yeo*

Micro/Nanophysics Research Laboratory, Monash University, Clayton, VIC 3800, Australia

(Received 26 January 2008; published 22 August 2008)

Spatiotemporal patterns form in many nonlinear physicochemical or biological systems. Although unusual, microfluidic systems are no exception. We observe such patterns to form by colloids along the free surface of a drop beneath which surface acoustic waves propagate, and propose fundamental mechanisms to elucidate their formation. With increasing excitation amplitude, the colloids first assemble into concentric rings and then cluster into islands due to a combination of capillarity and surface acceleration. As the excitation is further increased, fluid streaming commences within the drop, inducing a transient metastable state in which the system alternates between colloidal island formation on the quiescent drop surface and subsequent erasure due to local vortex generation.

DOI: 10.1103/PhysRevLett.101.084502 PACS numbers: 47.61.−k, 47.35.Rs, 47.54.−r, 47.57.J−

Sorting cells and biomacromolecules for point-of-care diagnostics and the patterning of nanostructured materials are among the many emerging applications of submicron colloidal particle assembly [1]. Given typically low Reynolds numbers and the associated flow stability due to the absence of inertial effects, it is unusual for microfluidic systems [2] to exhibit complex pattern formation characteristic of nonequilibrium physical systems [3]. Recently, however, a host of microfluidic manipulations driven *inertially* by MHz-order surface acoustic waves (SAWs)—nanometer amplitude undulatory waves that propagate across a solid surface—have been demonstrated [4–7]. The nonlinearities that appear from the acoustic irradiation inherent to the excitation method used in these studies may also be exploited to form complex and chaotic dynamic patterns, as demonstrated here with fascinating colloidal patterns that form on the free surface of a sessile liquid drop containing a colloidal suspension. We delineate the specific conditions under which a variety of patterns arise due to vibration excitation from SAWs traveling along the piezoelectric substrate on which the drop is placed.

SAWs, here as transverse axially polarized Rayleigh waves [8], are generated by applying a continuous sinusoidal electrical input into a nonweighted interdigital transducer (IDT, Al/Ti 25-finger pair electrode) patterned on the surface of a single-crystal piezoelectric substrate (127.68° *Y-X* cut lithium niobate, $LiNbO_3$, Roditi Ltd.) via standard UV photolithography. Given an IDT finger and gap width of 49 μm, the SAW wavelength $\lambda = 196$ μm and hence the resonant frequency $f = c/\lambda = 19.35$ MHz, where $c = 3788$ m/s is the sound velocity of the unloaded crystal surface. Further details of the SAW device and its fabrication may be found in prior work [4–7]. To avoid wave reflection from the device ends, polydimethylsiloxane (α-gel, Geltec Ltd.) was placed at both ends of the device as an effective wideband acoustic absorber. As shown in the inset of Fig. 1(a), a drop containing an aqueous suspension of 500 nm fluorescent polystyrene particles (Duke Scientific) with emission and excitation maxima at 508 nm and 468 nm, respectively, diluted to a concentration of 1.4×10^9 particles/ml, is placed on the substrate entirely within the SAW propagation path; the drop volume is altered to allow a range of drop diameters to be studied [Fig. 1(a)]. Because of the substrate hydrophilicity, the drop assumes a slender and flat shape with a contact angle of roughly 40°. Visualization of the particle and fluid motion was carried out using a high speed video camera (Olympus iSpeed) at 60 fps connected to a fluorescence stereomicroscope (Olympus BXFM) under reflected wideband blue light with emission centered at 462 nm. The power input to the IDT was monitored using wideband current and voltage probes (CT1 and P6114B, Tektronix) connected to a digital source oscilloscope (TDS4012B, Tektronix).

Figure 1(a) illustrates the various colloidal patterns that appear due to different choices of applied power and initial drop diameter, as seen from above. At relatively low power in regime A, the particles are observed to assemble into closely-spaced concentric rings that appear to coincide with the nodal lines of the standing wave pattern induced on the drop's free surface. This is supported by the fact that the ring separation, approximately 100 μm, is roughly half the SAW wavelength, suggesting that the standing wave induced on the free surface has the same frequency as the SAW on the substrate, a notion corroborated by fast fourier transform frequency spectra of the capillary wave vibration obtained using a laser doppler vibrometer (LDV, MSA-400, Polytec) [9]. By traversing the laser focal plane from the substrate to a plane just above the drop free surface, i.e., moving from left to right in Fig. 1(b) wherein the substrate and interface are indicated by vertical dashed lines, it is then possible to measure the frequency of the vibration on both the substrate and the free surface. Figure 1(b) shows

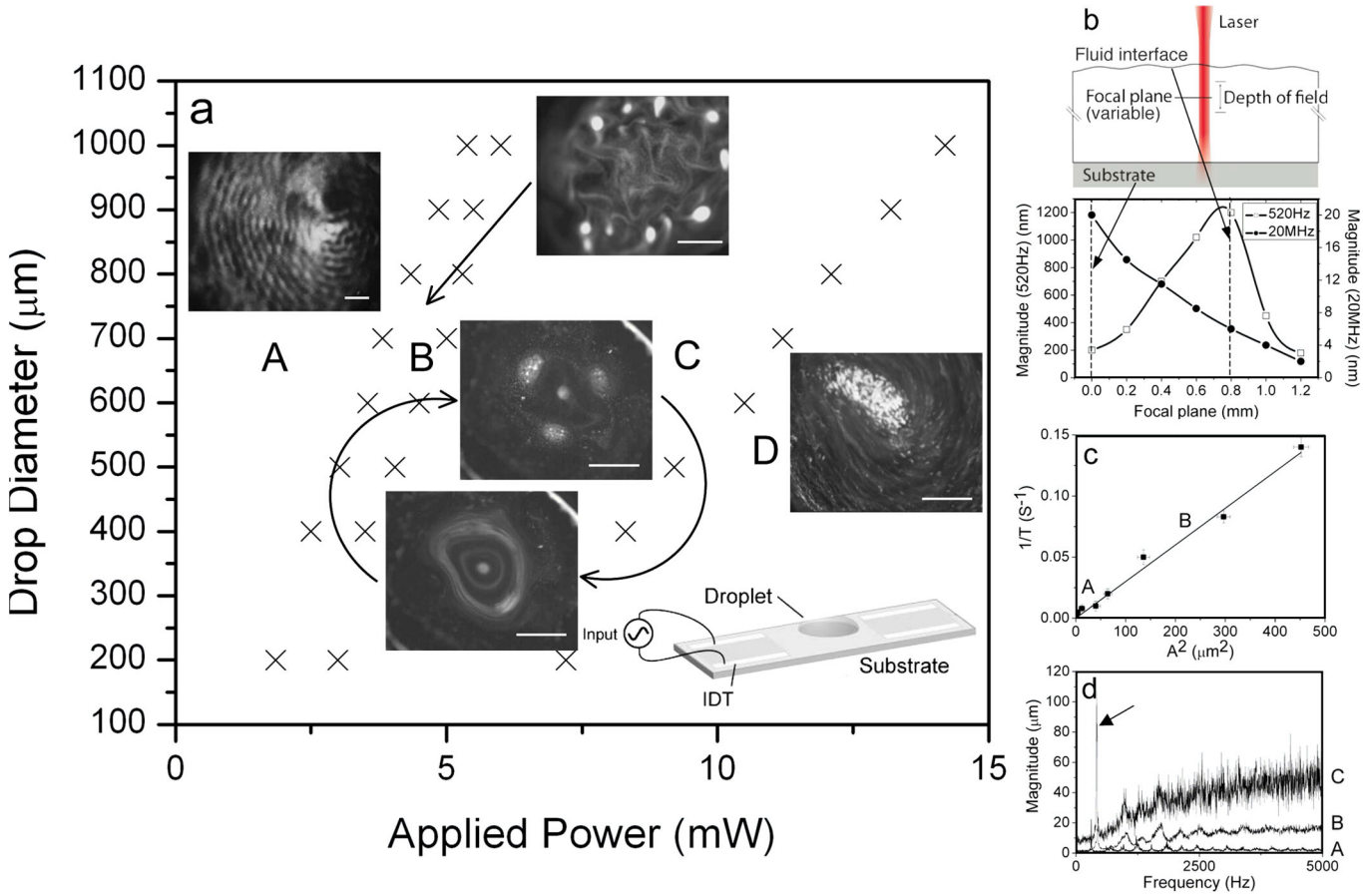

FIG. 1 (color online). (a) Map delineating the various patterns observed on the drop surface (from above) for different initial drop sizes and input powers. In regime A, particles drift into concentric rings due to high frequency (~20 MHz) interfacial standing waves induced by the SAW excitation. At higher powers, these particles cluster into islands about intersection points between high frequency linear nodal lines and the subharmonic (~1 kHz) circular nodal line from the fundamental capillary-viscous resonance (regime B). In regime C, particles alternately collect as islands under quiescent conditions and disperse due to local streaming vortices about antinodal positions. In regime D, all collection phenomena are overwhelmed by strong bulk streaming. (b) Wave vibration amplitudes measured at 520 Hz and 20 MHz using the LDV. The laser focal plane is shifted from the substrate to a plane just above the free surface (left to right, substrate and free surface indicated by vertical dashed lines—the data points away from the two dashed lines are irrelevant; the measurement tail to the right of the dashed line representing the free surface arises due to the dynamic oscillation of the drop and thus depends on the oscillation amplitude). Note that the focal depth of the laser plane, of order 200 μm, is significantly larger than the oscillation amplitudes, as illustrated in the schematic above. (c) Linear relationship between the inverse drift time for particles to migrate into the linear (regime A) and island (regime B) assemblies and the squared capillary wave amplitude. (d) Low frequency capillary vibration magnitudes for each regime (A–C) in (a). All scale bars are ~200 μm.

the existence of vibrations along the free surface possessing the same frequency (~20 MHz) as the 20 MHz SAW propagating along the substrate, albeit at a lower amplitude.

Hydrophillic (hydrophobic) particles are known to assemble along *nodal* (*antinodal*) points along a standing wave on the free surface of a vibrated liquid; this *drifting* process is driven by capillarity and interfacial acceleration which, together, result in a particle drift force along the interface that scales as the square of the wave amplitude A [10]. Balancing the drift force with the unsteady Stokes' drag in the high frequency limit $\frac{2}{3}\pi\rho a^3(du/dt) + 3\pi a^2 u(\rho\mu f)^{1/2} \sim \rho a^3 L/T + (\rho\mu f)^{1/2} a^2 L/T$ [11], where ρ is the fluid density, μ the fluid viscosity, u the fluid velocity, a the particle size, t the time, and, U, L and T are the characteristic velocity, length and time scales, respectively, it then follows that the inverse of the time taken for the particles to assemble into the ring structures $1/T$ scales as A^2, consistent with that observed [Fig. 1(c)]. Although the particles were homogeneously dispersed within the drop initially, instead of deposited onto the vibrating interface as in [10], a large number of particles nevertheless appeared to sit on the interface due to the slenderness of the drop, the hydrophobicity of the particles and the vibration at the interface.

Traversing horizontally from regime A to regime B in Fig. 1(a) through an increase in power for a fixed initial drop size, the particles originally gathered in the narrowly

spaced rings in regime A then cluster into islands in regime B. This change is accompanied by the appearance of low frequency subharmonic vibration on the drop free surface; Fig. 1(d) shows the LDV-measured surface vibration amplitude from 0–5 kHz for each regime in Fig. 1(a), indicating a broadband increase in the capillary wave amplitude as the power is increased.

Moreover, a strong resonance peak in the drop surface vibration amplitude appears near 500 Hz as the power is increased [indicated by the arrow in Fig. 1(d)], associated with the fundamental capillary-viscous resonance of the free drop [12]. Balancing capillary and viscous stresses, we obtain a capillary-viscous resonant frequency $f \sim \gamma/\mu R \sim 1$ kHz [12] close to that observed in Figs. 1(b) and 1(d); γ is the interfacial tension and R the drop dimension. The emergence of these large amplitude low frequency (1 kHz order) waves, in addition to the existing low amplitude high frequency (20 MHz) SAW-induced standing waves at the drop free surface, then lead to nodal *points* where the nearly straight nodal lines of the high frequency standing wave intersect with the single nodal circle of the subharmonically induced low frequency standing wave. Assuming potential flow in a two-dimensional axisymmetric drop, an expansion of the Laplace equation governing the streamfunction in cylindrical harmonics then yields a solution that corresponds to this fundamental radial axisymmetric mode, as illustrated in the inset of Fig. 2(a). Consequently, the particles drift from the linear concentric rings toward the nodal points once the low frequency capillary wave amplitude, negligible in regime A, approaches the amplitude of the high frequency waves. This is supported by the time required for the particles to migrate into these colloidal islands, which still scales as $1/A^2$ [Fig. 1(c)].

Curiously, the drop size defines the number of islands [Fig. 2(a)]. If the SAW excitation power were to be kept constant and the drop allowed to evaporate, thereby reducing its overall volume, the number of islands and their positions successively mutate with the progressive evaporation of the drop, as demonstrated in Fig. 2(b). In fact, the number of islands concomitantly decreases in a manner tightly bound to the radius of the drop as depicted by the successive images in Fig. 2(b) and in the movie (see movie 1 [9]). The caricatures beneath each image illustrate the shrinking nodal circle of the large amplitude low frequency capillary-viscous vibration, consistent with the Rayleigh-Lamb dispersion relationship [13], as it progressively overlaps fewer and fewer SAW-induced, fixed high frequency linear nodal lines, reducing the number of sites for particles to collect as time passes. The transition from one island arrangement to the next is rapid, and the position of the islands along the SAW propagation direction is not seen to shift, suggesting the importance of the SAW-induced standing waves in triggering the phenomena. Altogether, the evaporation behavior supports the postulated mechanism for the colloidal island formation.

At the high excitation amplitude end of the spectrum, i.e., regime D in Fig. 1(a), bulk liquid recirculation (*acoustic streaming*) within the drop occurs. In this regime, colloidal particles are rapidly drawn into the toroidal vortex that arises due to shear gradients [14] generated by streaming in the drop. The particles are drawn inwards along the substrate-drop interface and collect along this interface at the center of the drop and away from the drop's free surface [6]. As the power is increased further, the particle collection in the bulk at the bottom center may be dispersed due to overwhelming convective forces induced by the acoustically-driven flow, and the drop may be induced to move [4] or even atomize [7].

Most peculiar of all, regime C in Fig. 1(a) comprises a transient metastable region in which the phenomena of regimes B and D occur in a cyclic *blinking* [15,16] fashion. Characterized by broadband vibration of the free surface growing roughly as a square of the frequency over the

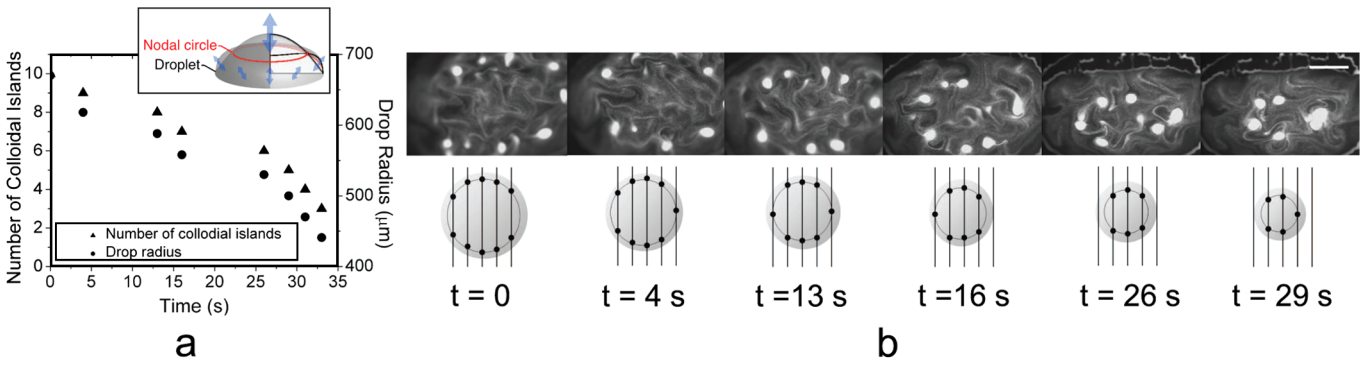

FIG. 2 (color online). Evaporation-driven mutation of the colloidal island assemblies (regime B). (a) The number of islands formed at nodal points decreases with the drop radius as it evaporates over time. (b) The bottom row depicts the number of islands based on the superposition of the nodal line of the high frequency SAW-induced free surface standing wave and the subharmonic capillary-viscous nodal circle, and their respective positions corresponding to the experimental images in the top row; note that the parallel lines are an idealization of the concentric rings in regime A of Fig. 1(a). The number of nodal intersections and therefore islands decrease as the drop evaporates and decreases in size. Scale bar ~200 μm.

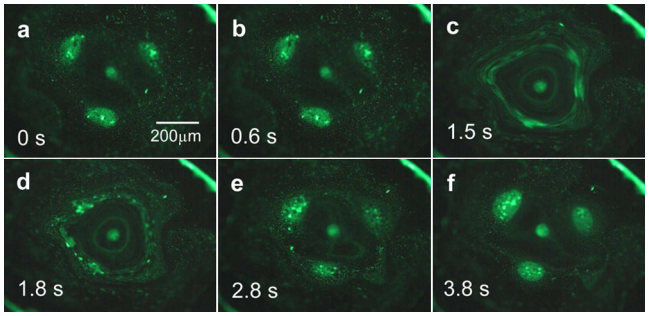

FIG. 3 (color online). Transient metastable transition region (regime C): Cyclic island formation and breakup process as a series of images acquired using high speed video microscopy at 60 fps. (a),(b) Colloidal island formation in the apparently quiescent fluid. (c),(d) Local streaming vortices at antinodal positions between the intersections of the low and high frequency standing waves disperses the particle assemblies. (e), (f) Reformation of the islands once streaming ceases.

range of capillary-viscous resonances [Fig. 1(d)], the behavior is a demonstration of the *fast* [17] excitation of the capillary-viscous resonances by the SAW, with SAW excitation at frequencies far higher than the resonance frequencies of the resonance phenomena itself.

As the cycle proceeds, the colloidal islands observed in Figs. 3(a) and 3(b) are erased due to strong local streaming vortices that appear about antinodal positions formed from a superposition of the low and high frequency standing waves appearing on the free surface [Figs. 3(c) and 3(d)]. After a short transient—the *blink*, the local streaming vortices cease and the islands reform under the apparently quiescent conditions [Figs. 3(e) and 3(f)]. The time required to complete each cycle varies in a statistically indeterminate fashion, and the direction of the vortices varies randomly from cycle to cycle. Furthermore, the particle trajectories drawn out from each island as the vortices begin to progressively intensify, diverge with a positive *Lyapunov exponent*, which suggests chaotic behavior [15]. A movie of the cycling best illustrates this extraordinary behavior (see movie 2 [9]).

Fast harmonic excitation combined with regular antinodal vortices are known to occur in fluid flows near critical symmetry-breaking bifurcations [16]. Here, a pair of equally probable solutions for either clockwise or counterclockwise rotation in the drop exists, controlled through an asymmetric particle concentration from one side of the drop to the other due to the presence of the islands. This results in particle collection behavior similar to that seen in laminar Couette flow characterized as a Hopf bifurcation arising as a consequence of spatial symmetry breaking [16]. Indeed the quasiperiodic behavior of the collection cycle in the intermediate regime (regime C) between the local and drop-wide collection characterized by regimes A and B, respectively, and the streaming-induced bulk concentration in regime D is a physically useful demonstration of chaotic Hopf bifurcation systems.

*leslie.yeo@eng.monash.edu.au

[1] G. M. Whitesides, J. P. Mathias, and C. T. Seto, Science **254**, 1312 (1991); E. Kim, Y. Xia, and G. M. Whitesides, Nature (London) **376**, 581 (1995).
[2] T. M. Squires and S. R. Quake, Rev. Mod. Phys. **77**, 977 (2005); J. El-Ali, P. K. Sorger, and K. F. Jensen, Nature (London) **442**, 403 (2006).
[3] T. Thorsen, R. W. Roberts, F. H. Arnold, and S. R. Quake, Phys. Rev. Lett. **86**, 4163 (2001).
[4] M. K. Tan, J. R. Friend, and L. Y. Yeo, Lab Chip **7**, 618 (2007).
[5] H. Li, J. R. Friend, and L. Y. Yeo, Biomaterials **28**, 4098 (2007).
[6] R. Shilton, M. K. Tan, L. Y. Yeo, and J. R. Friend, J. Appl. Phys. **104**, 014910 (2008).
[7] A. Qi, L. Y. Yeo, and J. R. Friend, Phys. Fluids **20**, 074103 (2008).
[8] Lord Rayleigh, Proc. London Math. Soc. **s1–17**, 4 (1885); H. Bateman, Proc. Natl. Acad. Sci. U.S.A. **24**, 315 (1938); R. M. White and F. W. Voltmer, Appl. Phys. Lett. **7**, 314 (1965).
[9] See EPAPS Document No. E-PRLTAO-101-034835 for (a) more information on laser Doppler vibrometry and (b) two movies on pattern formation dynamics. For more information on EPAPS, see http://www.aip.org/pubservs/epaps.html.
[10] D. Vella and L. Mahadevan, Am. J. Phys. **73**, 817 (2005); G. Falkovich, A. Weinberg, P. Denissenko, and S. Lukaschuk, Nature (London) **435**, 1045 (2005).
[11] L. D. Landau and E. M. Lifshitz, *Fluid Mechanics* (Pergamon, Oxford, 1959).
[12] L. Y. Yeo, D. Lastochkin, S.-C. Wang, and H.-C. Chang, Phys. Rev. Lett. **92**, 133902 (2004).
[13] H. Lamb, *Hydrodynamics* (Cambridge University Press, Cambridge, England, 1932); M. Strani and F. Sabetta, J. Fluid Mech. **141**, 233 (1984).
[14] D. Leighton and A. Acrivos, J. Fluid Mech. **181**, 415 (1987); L. Y. Yeo, D. Hou, S. Maheshswari, and H.-C. Chang, Appl. Phys. Lett. **88**, 233512 (2006).
[15] M. C. Cross and P. C. Hohenberg, Rev. Mod. Phys. **65**, 851 (1993).
[16] J. Langenberg, G. Pfister, and J. Abshagen, Phys. Rev. E **70**, 046209 (2004).
[17] J. S. Jensen, J. Fluids Struct. **11**, 327 (1997).